Semiconductor Laser Dynamics for Feedback from a Finite-Penetration-Depth Phase-Conjugate Mirror

David H. DeTienne, George R. Gray, Govind P. Agrawal, *Fellow, IEEE,* and Daan Lenstra

Abstract— Most of the previous treatments of semiconductor lasers subject to optical feedback from a phase-conjugate mirror (PCM) have assumed that the PCM responds instantaneously. Furthermore, the mechanism responsible for phase conjugation does not usually enter into the analysis. In this paper, we derive the time-dependent reflectivity of a PCM created through nondegenerate four-wave mixing in a Kerr-type nonlinear medium. The resulting laser dynamics are compared with the case of the ideal PCM, as a function of the external-cavity length, the PCM reflectivity, and the PCM interaction depth. The PCM with a significant interaction depth tends to suppress otherwise chaotic output and produces pulses whose repetition rate is tunable by varying PCM reflectivity. At high feedback levels, it stabilizes the laser output. We use the circle-map formalism to explain our numerical results.

Index Terms— Chaos, chaos control, optical feedback, pulses, semiconductor laser, tunable frequency.

I. INTRODUCTION

THE EFFECTS OF optical feedback on semiconductor lasers from a phase-conjugate reflector have been attracting considerable attention lately, due in part to the potential for creating ultrashort, mode-locked pulses [1]–[7]. Semiconductor lasers subject to phase-conjugate feedback (PCF) exhibit behavior which can differ radically from the case of conventional optical feedback (COF) [8], [9]. Some of these differences have been discussed for the case of a single-longitudinal-mode semiconductor laser [10]. However, the effects of PCF in multimode semiconductor lasers have not yet been fully explored. When a semiconductor laser oscillates in multiple longitudinal modes, PCF obtained through four-wave mixing can lead to mode locking and short-pulse output [1].

The theoretical modeling of PCF has generally assumed, for simplicity, that the phase-conjugate mirror (PCM) responds instantaneously to the incident radiation. This assumption is not generally valid when the PCM is constructed from a photorefractive crystal or by using an atomic vapor. For this reason, it is often assumed that the PCM is operating through four-wave mixing in a Kerr-type nonlinear medium with femtosecond response. What is not appreciated is that the PCM
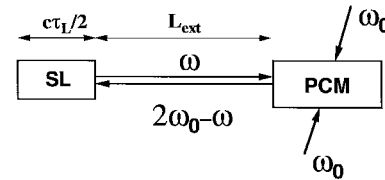
Fig. 1. Semiconductor laser (SL) obtaining feedback from a finite-interaction-depth PCM based on nondegenerate four-wave mixing pumped by a laser at ω_0.

does not respond instantaneously even for a Kerr medium since it takes time for light to traverse the nonlinear medium and to generate the phase-conjugated signal. The purpose of this paper is to take into account the finite propagation delay within the PCM and to demonstrate the resulting dynamics of a laser subject to feedback resulting from such a PCM. In particular, we show that such PCF can lead to pulsed output with tunable repetition rates, even though the laser current is constant.

II. MODEL

Earlier efforts to model PCF were done by a simple modification of the model used for COF. This approach is limiting, however, in several ways. A conventional mirror has a relatively flat spectral response, fast response time, and a thin interaction depth. A phase-conjugate mirror, by contrast, tends to have a peaked frequency response, a finite interaction depth, and may respond sluggishly [11]. In this work, we develop an improved model for PCF and show some interesting results from simulations. Fig. 1 shows the experimental diagram and parameters of interest.

For an instantaneously responding PCM, the simplest rate equations for a semiconductor laser subject to degenerate PCF are [6]

$$\frac{dN}{dt} = \frac{I}{q} - \frac{N}{\tau_e} - G|E(t)|^2 \tag{1}$$

$$\frac{dE}{dt} = \frac{1}{2}(1 - i\alpha)(G - \gamma)E(t) + \zeta + \kappa E^*(t - \tau). \tag{2}$$

In (1) and (2), N is the carrier population inside the active layer of the laser, I is the injected current, q the electron charge, and τ_e is the carrier lifetime. E is the laser's complex slowly varying electric field at the output facet. α is the linewidth enhancement factor (α was set equal to 3 for this work). G is the gain which is defined as $G = G_N(N - N_0)$, where G_N and N_0 are the gain derivative and transparency carrier number, respectively, and γ is the loss. ζ accounts for nonlinear gain and for intrinsic four-wave mixing processes

[12]. In this work, only nonlinear gain was considered. τ is the round-trip time in the external cavity, $\tau = 2L_{\text{ext}}/c$, where L_{ext} is the distance from the laser to the PCM. κ is the feedback rate, a measure of the reflectivity of the PCM. In analogy with conventional feedback, the feedback rate κ in this simple model is written as

$$\kappa = \frac{(1 - r_2^2)}{\tau_L} \frac{r_3}{r_2} \qquad (3)$$

where r_2 is the field reflectivity of the laser output facet, τ_L is the round-trip time inside the solitary laser, and r_3 is the field reflectivity of the PCM, including any coupling losses back into the laser. In this work, $r_2^2 = 0.12$ and $\tau_L = 9.3$ ps. The PCF term, as in the case of ordinary feedback, depends on the field at one round trip earlier, time τ. In contrast to COF, however, the field is conjugated by the PCM. Equations (1) and (2) are integrated in the weak-feedback regime, so multiple round-trip reflections can be neglected. The laser is assumed to operate in just one longitudinal mode. The results shown in this paper are deterministic in nature, since no noise terms are included in (1) and (2).

Equation (2) shows the idealized case where the feedback comes from an instantaneously responding PCM. The PCF term, $E^*(t - \tau)$, gives the feedback from just one round-trip time τ earlier. The starting point for an improved PCF model is to write the laser field as a Fourier integral in the form

$$E(t) = \frac{1}{2\pi} \int_{-\infty}^{+\infty} A(\omega) \exp[i(\omega - \omega_L)t] \, d\omega \qquad (4)$$

where $A(\omega)$ is the Fourier component and ω_L is the frequency at which the laser spectrum is centered. It is useful to rewrite (4) relative to the PCM pump frequency ω_0. By defining a "bulk" detuning $\delta_0 = \omega_L - \omega_0$, where ω_0 is the frequency of the pump laser used for four-wave mixing, and $x \equiv \omega - \omega_0$ as the relative detuning, (4) can be written as

$$E(t) = \frac{1}{2\pi} \exp(-i\delta_0 t) \int_{-\infty}^{+\infty} A(x) \exp(ixt) \, dx. \qquad (5)$$

A frequency component $A(\omega)$ of the incident field, detuned by δ from the pump frequency, is reflected by the PCM as [13]

$$E_{pc}(\omega) = r_{\text{pcm}}(\omega) A^*(\omega) \exp[i(\omega_0 - \delta)t] \exp(i\delta\tau). \qquad (6)$$

Our improved PCF model is then obtained by combining (5) and (6):

$$\boxed{\begin{aligned} E_{pc}(t) = \frac{1}{2\pi} \exp(-i\delta_0 t) \int_{-\infty}^{+\infty} r_{\text{pcm}}(x) A^*(x) \\ \cdot \exp[-ix(t - \tau)] \, dx. \end{aligned}} \qquad (7)$$

Equation (7) is a main result of the paper. $E_{pc}(t)$ represents the feedback field due to reflection from the PCM. The physics of the PCM mechanism is contained in the field reflectivity r_{pcm}, which is generally frequency dependent.

As an important application of (7), we consider the case where the PCM is constructed by nondegenerate four-wave mixing in a fast nonlinear medium, such as a Kerr medium.

For this case, the well-known expression for the frequency-dependent reflectivity is given by [14]

$$r_{\text{pcm}}(\omega) = \frac{-i\Gamma \, \tan(\beta L_m)}{\beta - (i\Delta k/2) \, \tan(\beta L_m)} \qquad (8)$$

where $\Gamma(1/m)$ is proportional to $\chi^{(3)}$ and the pump power, $\beta \approx \sqrt{\Gamma^2 + (\Delta k/2)^2}$, L_m is the PCM interaction length, and Δk is the wavenumber mismatch between the pump frequency ω_0 and probe frequency ω. The equations are simplified if a parameter t_m is defined as

$$t_m \equiv \frac{n \tan(\beta L_m)}{\beta c} \qquad (9)$$

where n is the refractive index of the PCM material and c is the speed of light in vacuum. It is often true experimentally that βL_m is small, so that, physically, t_m is approximately the time it takes the light to penetrate the PCM ($t_m \approx nL_m/c$). With this definition, the phase-conjugate reflectivity can be written as

$$r_{\text{pcm}}(x) = \frac{\Gamma}{n} \frac{t_m}{t_m \, x + i}. \qquad (10)$$

It is important to stress that (8) and (10) are obtained for a PCM whose material response time is instantaneous (the Kerr nonlinearity, for example). The penetration time t_m is a measure of the time it takes for the laser beam to penetrate inside the PCM in order to build the phase-conjugate reflection; thus t_m is related to the effective depth or length of the PCM. If an atomic or photorefractive medium is used for a PCM, the material's response time will also need to be included.

To complete the model, (10) is substituted into (7) and the integration is performed by contour integration. For simplicity, the frequency dependence of t_m is neglected. The signal reflected from the PCM is then given by

$$E_{pc}(t) = \frac{-i\Gamma c}{n} \exp(-i\delta_o t) \int_{-\infty}^{t} E^*(t' - \tau) \\ \cdot \exp\left[-i\delta_o(t' - \tau) - \frac{(t - t')}{t_m}\right] dt' \qquad (11)$$

where the integral occurs due to expressing the result in terms of $E^*(t' - \tau)$ using an inverse Fourier transform based on (4). The upper integration limit in (11) has been replaced by t, since the conjugated field cannot depend on future times.

To include the result (11) into the rate equation (2), we multiply as usual by $(1 - r_2^2)/(\tau_L r_2)$ so that the new rate equation becomes

$$\frac{dE}{dt} = \frac{1}{2}(1 - i\alpha)(G - \gamma)E(t) + \frac{\kappa}{t_m} \exp[-2i\delta_0(t - \tau/2)] \\ \cdot \int_{-\infty}^{t} E^*(t' - \tau) \exp\left[-\frac{(1 - i\delta_0 t_m)(t - t')}{t_m}\right] dt'. \qquad (12)$$

If we assume zero detuning ($\delta_0 = 0$) and take the limit as t_m approaches 0, then (12) reduces to (2). In addition to a new rate equation, this analysis has also provided the feedback rate in terms of the four-wave mixing parameters:

$\kappa = (-i\Gamma c/n)(1 - r_2^2)/(\tau_L r^2)t_m$, or in terms of the effective PCM reflectivity r_3: $r_3 = (-i\Gamma c/n)t_m$.

Numerically, (12) is very inefficient to apply directly, since it requires solving the feedback integral at each time step Δt. Moreover, separating (12) into two separate equations, the standard method for reducing higher order differential equations into a system of first-order equations, leads to an ill-posed problem. Fortunately, we were able to come up with an efficient recursive definition for the feedback integral with (11) as the starting point. The recurrence relation is

$$E_{pc}(t) = E^*(t - \Delta t/2 - \tau)\exp(-\Delta t/2t_m)\Delta t$$
$$+ \exp(-\Delta t/t_m)E_{pc}(t - \Delta t). \tag{13}$$

The first term is a rectangle approximation for the most recent Δt (valid since the numerical time steps are small), and the second term gives everything previous. This recursive definition is numerically efficient, only adding linearly to the computational effort. The usual method of adding an additional first-order differential equation to eliminate the integral adds significantly more overhead as the order of operations scales as the number of differential equations squared [15].

III. SIMULATION RESULTS

With a simulated system, the parameter space that can be searched is huge, as any parameter in the underlying set of equations can be varied. Physically, not every parameter can be varied by turning a knob in the laboratory (the value of α, for instance). We chose to vary the penetration depth of the PCM $(t_m$, which can be controlled by the choice of PCM, the physical size, or the diameters of the pump beams [16]), the field reflectivity of the PCM (r_3), and the external cavity length (L_{ext}). All of these parameters can be varied experimentally.

An important tool for searching the parameter space is the bifurcation diagram [17]. The bifurcation diagrams tell at a glance the state of the system for a range of bifurcation variable values. Where there are no points in the bifurcation diagram, the system is stable. Where a single point exists for a particular value of the bifurcation variable (r_3 for this paper), the laser is pulsing at one dominant frequency (period-one bifurcation). Where there are two points, the laser exhibits period doubling, etc. A filled-in area indicates oscillations at many frequencies or chaos.

A. Effect of Finite Interaction Depth

First, we investigate the effect of PCM interaction depth by changing the parameter t_m, so we can see how our improved rate equations differ from those of an ideal PCM. We assume operation close to threshold $(I/I_{th} = 1.05)$, and an external cavity spacing $L_{ext} = 10$ cm. Fig. 2(a) shows a bifurcation diagram, with reflectivity as the bifurcation variable, for the instantaneous PCM, that is $t_m = 0$ ns. Also shown in Fig. 2(a) are the average power and the standard deviation of the power. There is a one-to-one correspondence between the chaotic regions in the bifurcation diagram and a large standard deviation, as expected.
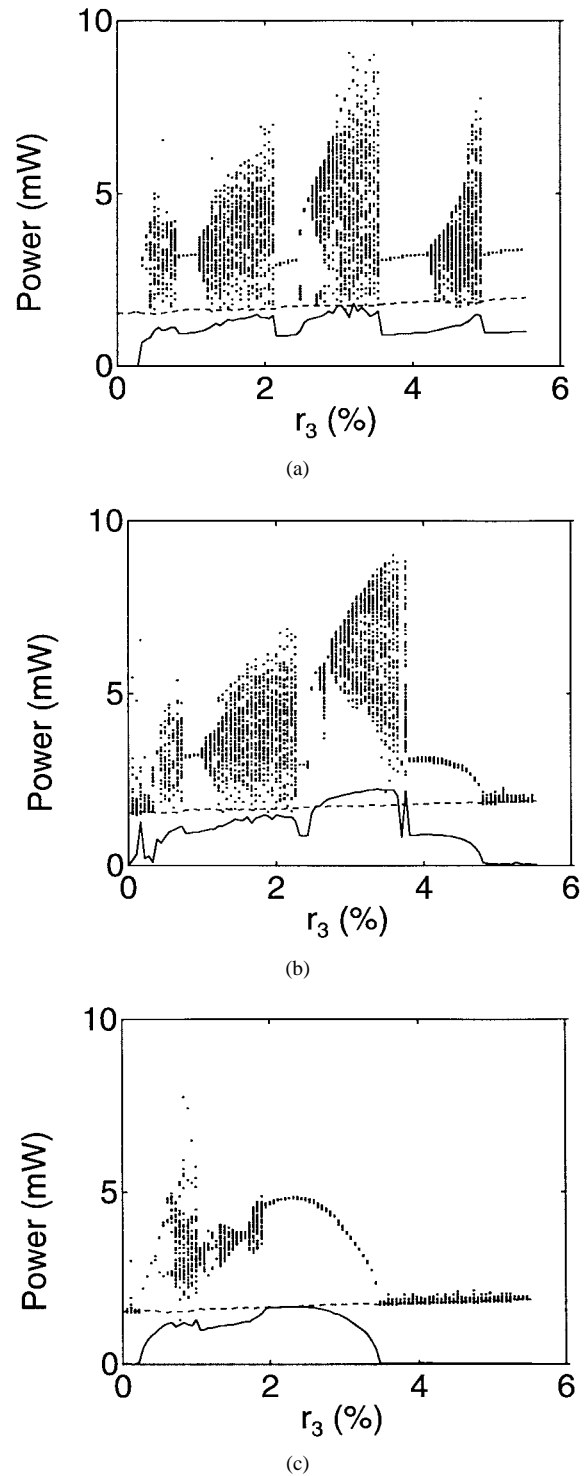
Fig. 2. (a) Bifurcation diagram ($\cdots$) of the laser power for $L_{ext} = 10$ cm as function of PCM field reflectivity for the ideal PCM $(t_m = 0$ ns). Also shown are the average power (- - - - -) and the standard deviation of the power (———). (b) Same as (a) except $t_m = 0.1$ ns. (c) Same as (a) except $t_m = 0.4$ ns.

Fig. 2(b) shows the same system but for a PCM with a penetration time $t_m = 0.1$ ns. This value is small compared to the relaxation-oscillation period $(T = 1.3$ ns). For low feedback levels $(r_3 < 3\%)$, the bifurcation diagrams are similar. However, as the feedback level is increased above $r_3 > 4.5\%$, the long mirror tends to suppress the chaos to the point that the
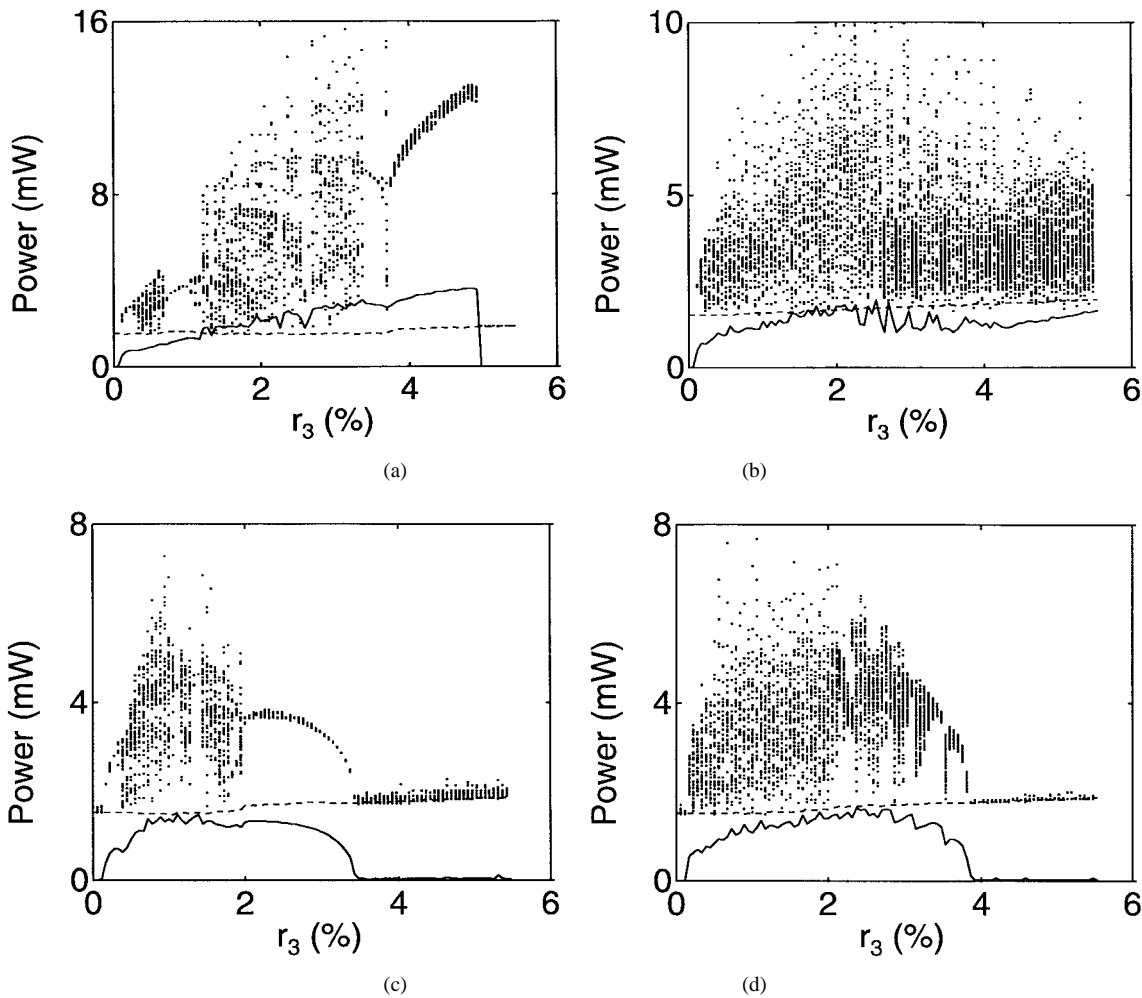
Fig. 3. (a) Same as Fig. 2(a) except $L_{\text{ext}} = 1$ cm. (b) Same as Fig. 2(a) except $L_{\text{ext}} = 100$ cm. (c) Same as Fig. 2(a) except $t_m = 0.4$ ns and $L_{\text{ext}} = 1$ cm. (d) Same as Fig. 2(a) except $t_m = 0.4$ ns and $L_{\text{ext}} = 100$ cm.

laser becomes nearly stable for $r_3 > 5\%$. This is easily seen as the power standard deviation is close to zero.

For Fig. 2(c), the penetration time of the mirror has been increased to $t_m = 0.4$ ns. A comparison of Fig. 2(a)–(c) shows that the chaos has now been virtually eliminated. In the range of $1.7\% < r_3 < 3.3\%$, the laser shows periodic behavior. For $3.3\% < r_3 < 11\%$, the laser operates stably (11% field or 1% power reflectivity was the cautious limit of validity set for the single-round-trip simulations). This behavior can be understood by inspection of (12). Basically, the integral performs a weighted averaging of the feedback. A greater t_m smooths the feedback more, leading to less chaos. Also, higher frequencies are attenuated more than lower frequencies, which would explain the tendency for period-one behavior for the long mirror. A quantitative description for this behavior will follow in Section IV.

B. Effect of External-Cavity Spacing

Changing the external-cavity length can have profound effects on the dynamics of the laser system. For $L_{\text{ext}} = 1$, 10, and 100 cm, Figs. 3(a), 2(a), and 3(b), respectively, show that for the instantaneous PCM case, changes in cavity length modify the bifurcation diagrams substantially. In general, as L_{ext} increases, the widths of the chaotic and nonchaotic windows decrease. For the case of $L_{\text{ext}} = 100$ cm, the windows are so narrow that it appears to be continuously chaotic. This behavior is similar to that of ordinary feedback [10], [18].

The effect of external-cavity length is less pronounced for a long PCM, with $t_m = 0.4$ ns. Figs. 3(c), 2(c), and 3(d) show, respectively, the bifurcation diagram for $L_{\text{ext}} = 1$, 10, and 100 cm. There is some tendency at weak feedback for there to be more chaos as Lext is increased, but regardless of L_{ext}, the chaos always ends at about $r_3 = 4\%$, and the envelopes of the bifurcation points are similar. So while the external-cavity length usually has a large effect on the laser dynamics, for the case of the long PCM it is a secondary effect. The dynamics are dominated by the PCM. The instantaneous PCM dynamics tend to scale with $\kappa\tau$ (in other words, $r_3\tau$, where $\tau = $ external round-trip time). The long PCM dynamics tend to scale with just κ or r_3. A circle-map explanation for these effects will be provided in Section IV.

C. Pulsed Operation

One interesting result from using a long PCM is that the laser can produce pulses, even though the injection current
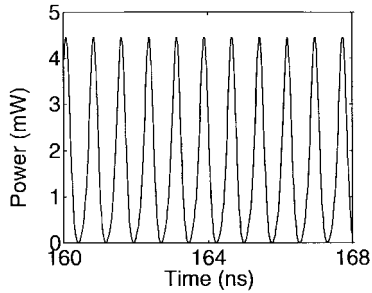
Fig. 4. 1.3-GHz pulsed operation. $t_m = 0.4$ ns, $L_{\text{ext}} = 10$ cm, and $r_3 = 2.5\%$.

is kept constant; an example is shown in Fig. 4. It is desirable to know which parameters and ranges of parameter values produce pulsed behavior, but a search for regions of pulsed operation can be tedious. A brute-force method such as viewing power verses time plots or doing Fourier transforms over a large parameter space is costly both in terms of human and computer time. However, the task is simplified by making use of the sampling performed in calculation of the bifurcation diagrams. The bifurcation diagrams are constructed by interpolating for the value of P ($|E|^2$, photon number) whenever N crosses the average-N plane in the direction of decreasing N. Thus, for simple periodic behavior, the sampling of P will occur at nearly the same point in each cycle. Thus, if we record this sampling frequency and compute its standard deviation (for little additional overhead), we can use this variable in conjunction with the standard deviation of the power and the power bifurcation diagram to determine not only the presence of periodic behavior but also the frequency of oscillation. For example, for period-one behavior, the power bifurcation diagram yields a single line with a large standard deviation. The sampling variable frequency, however, gives the frequency of oscillation when its standard deviation is small. Fig. 4 is a typical picture seen for regions of pulsed operation for the long PCM, showing a repetition rate of 1.3 GHz. Note that the pulses have a 100% modulation depth.

Fig. 5(a) and (b) show the sampling frequency verses feedback for an instantaneous PCM and a deep PCM, respectively. The instantaneous PCM tends to show regions of periodic behavior (small standard deviation of sampling frequency and a line indicating period-one behavior on the power bifurcation diagram, Fig. 2a). The equal frequency spacing of 1.5 GHz (the external round-trip frequency) indicates a locking behavior between the relaxation oscillations and the round-trip frequency ($1/\tau = 1.5$ GHz). Note that these frequency-locking regions are absent for the long PCM, Fig. 5(b), yet another indicator that the long PCM is dominating the dynamics rather than the external-cavity round-trip frequency effects. Also, the instantaneous PCM shows much higher frequencies (up to 6 GHz) than the long PCM (< 1.5 GHz). As mentioned before, inspection of (12) shows that the long PCM tends to filter out higher frequencies.

IV. CIRCLE MAP

A circle map is a useful tool for understanding systems that have two frequencies that may lock together. It can be used

(a)

(b)
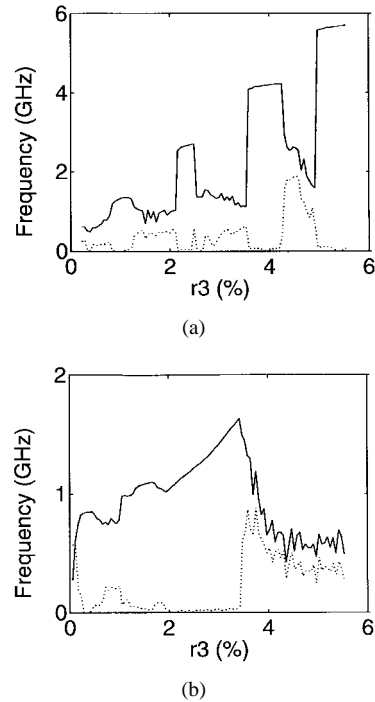
Fig. 5. (a) Average bifurcation sampling frequency (———) as a function of feedback for $t_m = 0$ ns, $L_{\text{ext}} = 10$ cm, and $r_3 = 2.5\%$. Also shown is the standard deviation of the bifurcation sampling frequency (———). (b) Same as Fig. 5(a) except $t_m = 0.4$ ns.

to predict the frequency-locking ratio, the onset of chaos, and whether a period-doubling route to chaos will be followed. A good tutorial on the circle map is found in [19]. The standard sine circle map is given by [19]

$$\theta(t + \Delta) = \theta(t) + 2\pi\Omega - r \sin[\theta(t)]. \tag{14}$$

Δ gives the period for one of the frequencies. The second frequency is given by $d\theta/dt$. Ω controls the frequency locking ratio. For $r = 0, \theta$ increases linearly with t, so that no locking can occur. For $r > 0, r \sin \theta$ provides a "restoring force" that allows the two frequencies to lock together in integer ratios for certain ranges of Ω and r values (the range of values for a particular locked frequency ratio is known as an Arnol'd Tongue). $r > 1$ is a necessary condition for chaos to exist.

A. Circle Map for PCF

The standard sine circle map does not apply directly to our system. A similar circle map can be derived, however, and circle-map techniques can be used to advantage. First, a sinusoidally oscillating E field is assumed:

$$E = E_{ss} + A \exp[-i\theta(t)] \tag{15}$$

where E_{ss} is the steady-state solution to (2), and A is the constant amplitude of the oscillation. In general, θ is not the phase of the E field, but rather gives the oscillation frequency ($\theta \cong \omega t$). This form gives a sinusoidal power oscillation, $P \sim EE^* = |E_{ss}|^2 + A^2 + 2|E_{ss}|A \cos \theta$.

By taking a time derivative of (15), equating its imaginary parts with (2), and realizing E_{ss} is the zero solution for (2),

a rate equation for θ results:

$$\frac{d\theta}{dt} = \frac{\alpha}{2}(G - \gamma) - \kappa \sin[(\theta(t - \tau) + \theta(t)].\qquad(16)$$

As $\theta \sim \omega t$, the argument to the sine term can be simplified:

$$\theta(t - \tau) + \theta(t) \sim 2\theta(t) - \omega\tau.\qquad(17)$$

If the derivative is approximated by a finite difference

$$\frac{d\theta}{dt} \approx \frac{\theta(t - \tau) - \theta(t)}{\tau}\qquad(18)$$

then (16) can be cast into a circle-map form:

$$2\theta(t + \tau) \approx 2\theta(t) + \alpha\tau(G - \gamma) - 2\kappa\tau\{\sin[2\theta(t)]\cos(\omega\tau)$$
$$- \cos[2\theta(t)]\sin(\omega\tau)\}.\qquad(19)$$

For deep PCF, the derivation starts with (12) and results in

$$2\theta(t + \tau) \approx 2\theta(t) + \alpha\tau(G - \gamma) - 2\frac{\kappa\tau}{\sqrt{1 + (\omega t_m)^2}}$$
$$\cdot \{\sin[2\theta(t)]\cos[\omega\tau + \arctan(\omega t_m)]$$
$$- \cos[2\theta(t)]\sin[\omega\tau + \arctan(\omega t_m)]\}.\qquad(20)$$

B. Onset of Chaos

Typically, the onset of chaos in lasers is predicted using a small-signal stability analysis [20]–[23]. Using the circle map has the advantage that small signals are not a necessary assumption (indeed, the amplitude does not even appear in the standard sine circle map). In (19) and (20), the term with $\kappa\tau$ can be used to predict the onset of chaos. Numerical solutions to (19) go multiperiodic and chaotic at $\kappa\tau \approx 1$, or equivalently $r_3 \approx 0.5$. Fig. 2(a) shows this circle-map value is close to the numerically simulated system. For the deep mirror, the onset of chaos occurs when

$$2\frac{\kappa\tau}{\sqrt{1 + (\omega t_m)^2}} > 1.\qquad(21)$$

As displayed in Fig. 5(b), there exists a linear relation between ω and $\kappa\tau$ for the deep mirror. Using this linear relation, (21) then can be solved for the case of $t_m = 0.4$ ns to show the onset of chaos to be about at $\kappa\tau \approx 0.75$, or equivalently $r_3 \approx 0.4$, which is very close to the value found from simulation of the full equations, as shown in Fig. 2(c). Also, in general, as $\kappa\tau$ increases, the likelihood for chaos is increased. With (21), however, this term tends to become constant with increasing ω; ω tends to vary linearly with κ, meaning that chaos does *not* become more likely with larger $\kappa\tau$ values. Stated another way, even though the mirror reflectivity is increased, the effective reflection remains the same! For all the deep mirror bifurcation diagrams [Figs. 2(b)–(c) and 3(c)–(d)], the system becomes stable at about $r_3 = 3.6\%$ and remains stable thereafter. This is in sharp contrast with the instantaneous mirror.

C. Windows of Chaos

Another interesting effect the circle map explains are the windows of chaos that appear in the instantaneous mirror bifurcation diagrams. Equation (19) has frequency-locking plateaus because the $\sin(2\theta)$ term provides a restoring force that keeps the system frequency locked over a range of $\kappa\tau$ values. The $\cos(2\theta)$ term does not provide a locking force. This leads to a mathematical (necessary) condition for locking:

$$\cos(\omega\tau) > |\sin(\omega\tau)|.\qquad(22)$$

In other words, locking is possible only when the feedback term is $\sin(2\theta)$ dominant. Recalling that τ is the round-trip time, (22) shows the circle map will be sine dominant, and hence locking is possible, whenever ω hits a harmonic of the round-trip frequency. Marked transitions in dynamic behavior may occur when the sine dominance changes to cosine dominance. For example, the system may go from chaos to sinusoidal behavior, as will be illustrated. For $L_{\text{ext}} = 10$ cm, the round-trip frequency $1/\tau$ and harmonics are 1.5, 3.0, 4.5, 6.0, etc., GHz. This corresponds well to Figs. 2(a) and 5(a). Equation (22) also shows that if ω varies linearly with κ or r_3, locking will be allowed over 1/4 of the r_3 range. Once again, this is illustrated by Figs. 2(a) and 5(a).

For the cases of $L_{\text{ext}} = 1$ cm, (22) shows that the spacing between the chaos and locking windows in the bifurcation diagram [Fig. 3(a)] will be 10 times larger than for the $L_{\text{ext}} = 10$ cm case, as the external cavity round-trip time τ is 10 times larger. Similarly, for $L_{\text{ext}} = 100$ cm, the chaos windows spacing will be 1/10 as large as for the $L_{\text{ext}} = 10$ cm case. This is illustrated in Fig. 3(b), where the windows are so finely spaced they appear to be continuous. The rule of thumb for laser feedback dynamicists has been that the "chaos scales with $\kappa\tau$." Often bifurcation diagrams for different L_{ext} values use $\kappa\tau$ as the bifurcation variable, as then the dynamics will look similar despite the differences in L_{ext}. The circle map quantifies the assertion that chaos scales with $\kappa\tau$.

For the deep PCM, the condition for having a sine dominant circle map is

$$\cos[\omega\tau + \arctan(\omega t_m)] > |\sin[\omega\tau + \arctan(\omega t_m)]|.\qquad(23)$$

Solving (23) for the case $t_m = 0.4$ ns, a transition from sine dominant to cosine dominant occurs at $r_3 \approx 3.3\%$. This analytical result is remarkably close to the transition from pulsed operation to stable operation, given by the full simulations, as can be seen from Figs. 2(c) and 5(b).

V. SUMMARY

We have derived the phase-conjugate feedback term that arises due to the finite interaction depth of a PCM operating through nondegenerate four-wave mixing. The new feedback term was numerically implemented with an efficient numerical algorithm. We found that the deep PCM tends to suppress chaos and higher frequencies, when the penetration time t_m becomes comparable to the relaxation-oscillation period. Locking between the relaxation-oscillation and the external round-trip frequencies is absent with the long PCM. It removes much of

the external-cavity spacing dependence in the laser dynamics. Regions with good pulses were found, with the pulse repetition rate being linearly tunable by varying the feedback level. An explanation for transitions from chaos to periodic operation, and hence an explanation for the spacing of the chaotic verses periodic windows in the bifurcation diagrams, was derived with the help of the circle-map formalism. This analysis also demonstrated that the deep PCM does not increase the likelihood for chaos even when its reflectivity is increased.

ACKNOWLEDGMENT

REFERENCES

[1] G. R. Gray, D. H. DeTienne, and G. P. Agrawal, "Mode locking in semiconductor lasers by phase-conjugate optical feedback," *Opt. Lett.,* vol. 20, pp. 1295–1297, June 1995.
[2] G. P. Agrawal and J. T. Klaus, "Effect of phase-conjugate feedback on semiconductor laser dynamics," *Opt. Lett.* vol. 16, pp. 1325-1327, 1991.
[3] G. H. M. van Tartwijk, H. J. C. van der Linden, and D. Lenstra, "Theory of a diode laser with phase-conjugate feedback," *Opt. Lett.* vol. 17, pp. 1590–1592, Nov. 1992.
[4] S. Mailhot and N. McCarthy, "Influence of phase conjugate optical feedback on the emission properties of visible low-power diode lasers," *Can. J. Phys.,* vol. 71, pp. 429–433, 1993.
[5] T. Shimura, M. Tamura, and K. Kuroda, "Injection locking and mode switching of a diode laser with a double phase-conjugate mirror," *Opt. Lett.,* vol. 18, pp. 1645–1647, 1993.
[6] G. P. Agrawal and G. R. Gray, "Effect of phase-conjugate feedback on the noise characteristics of semiconductor lasers," *Phys. Rev. A,* vol. 46, pp. 5890–5898, Nov. 1992.
[7] N. Cyr, M. Breton, M. Tetu, and S. Theriault, "Laser-diode frequency control by resonant phase-conjugate reflection from an atomic vapor," *Opt. Lett.* vol. 16 pp. 1298–1300, Sept. 1991.
[8] R. W. Tkach and A. R. Chraplyvy, "Regimes of feedback effects in 1.5-μm distributed feedback lasers," *J. Lightwave Technol.,* vol. LT-4, pp. 1655–1661, 1986.
[9] G. H. M. van Tartwijk and D. Lenstra, "Semiconductor lasers with optical injection and feedback," *Quantum Semiclass. Opt.* vol. 7, pp. 87–143, 1995.
[10] G. R. Gray, D. Huang, and G. P. Agrawal, "Chaotic dynamics of semiconductor lasers with phase-conjugate feedback," *Phys. Rev. A,* vol. 49, pp. 2096–2105, 1994.
[11] D. H. DeTienne, G. R. Gray, G. P. Agrawal, and D. Lenstra, "Semiconductor laser coupled to a finite-response time phase-conjugate mirror," *Proc. SPIE,* vol. 2693, pp. 689–700, 1996.
[12] G. R. Gray and G. P. Agrawal, "Importance of self-induced carrier-density modulation in semiconductor lasers," *IEEE Photon. Technol. Lett.,* vol. 4, pp. 1216–1219, Nov. 1992.
[13] G. H. M. van Tartwijk and D. Lenstra, "Semiconductor lasers with optical injection and feedback," *Quantum Semiclass. Opt.*, vol. 7, pp. 87–143, 1995.
[14] D. M. Pepper and A. Yariv, *Optical Phase Conjugation,* R. A. Fisher, Ed.   New York: Academic, 1983.
[15] F. Acton, *Numerical Methods that Work.*   New York: Harper & Row, 1970.
[16] R. W. Boyd, *Nonlinear Optics.*   New York: Academic, 1992, ch. 6.
[17] J. Mørk, B. Tromborg, and J. Mark, "Chaos in semiconductor lasers with optical feedback: Theory and experiment," *IEEE J. Quantum Electron.,* vol. 28, pp. 93–108, 1992.
[18] A. T. Ryan, G. P. Agrawal, G. R. Gray, and E. C. Gage, "Optical-feedback-induced chaos and its control in multimode semiconductor lasers," *IEEE J. Quantum Electron.,* vol. 30, pp. 668–679, Mar. 1994.
[19] J. Glazier and A. Libchaber, "Quasiperiodicity and dynamical systems: An experimentalist's view," *IEEE Trans. Circuits Syst.,* vol. 35, pp. 790–809, July 1988.
[20] J. Helms and K. Petermann, "Simple analytic expression for the stable operation of laser diodes with optical feedback," *IEEE J. Quantum Electron.,* vol. 26, pp. 833–836, May 1990.
[21] B. Tromborg and J. Mørk, "Stability analysis and the route to chaos for laser diodes with optical feedback," *IEEE Photon. Technol. Lett.,* vol. 2, pp. 549–552, Aug. 1990.
[22] A. Ritter and H. Haug, "Theory of laser diodes with weak optical feedback, I. Small-signal analysis and side-mode spectra," *J. Opt. Soc. Amer. B,* vol. 10, pp. 130–144, Jan. 1993.
[23] ———, "Theory of laser diodes with weak optical feedback. II. Limit-cycle behavior, quasiperiodicity, frequency locking, and route to chaos," *J. Opt. Soc. Amer. B,* vol. 10, pp. 145–154, Jan. 1993.

David H. DeTienne, photograph and biography not available at the time of publication.

George R. Gray, photograph and biography not available at the time of publication.

Govind P. Agrawal (M'83–SM'86–F'96), for photograph and biography, see p. 468 of the March 1997 issue of this JOURNAL.

Daan Lenstra, photograph and biography not available at the time of publication.